Energy transfer in Eu^{3+} doped scheelites: use as thermographic phosphor

Katrien W. Meert,[1,2] Vladimir A. Morozov,[3,4] Artem M. Abakumov,[3] Joke Hadermann,[3] Dirk Poelman,[1,2] and Philippe F. Smet[1,2,*]

[1]*LumiLab, Department of Solid State Sciences, Ghent University, Krijgslaan 281-S1, 9000 Ghent, Belgium*
[2]*Center for Nano- and Biophotonics (NB-Photonics), Ghent University, B-9000, Belgium*
[3]*EMAT, University of Antwerp, Groenenborgerlaan 171, Antwerp B-2020, Belgium*
[4]*Chemistry Department, Moscow State University, 119991 Moscow, Russia*
[*]*philippe.smet@ugent.be*

Abstract: In this paper the luminescence of the scheelite-based $CaGd_{2(1-x)}Eu_{2x}(WO_4)_4$ solid solutions is investigated as a function of the Eu content and temperature. All phosphors show intense red luminescence due to the $^5D_0 - {}^7F_2$ transition in Eu^{3+}, along with other transitions from the $^5D_1$ and $^5D_0$ excited states. For high Eu^{3+} concentrations the intensity ratio of the emission originating from the $^5D_1$ and $^5D_0$ levels has a non-conventional temperature dependence, which could be explained by a phonon-assisted cross-relaxation process. It is demonstrated that this intensity ratio can be used as a measure of temperature with high spatial resolution, allowing the use of these scheelites as thermographic phosphor. The main disadvantage of many thermographic phosphors, a decreasing signal for increasing temperature, is absent.

OCIS codes: (160.2540) Fluorescent and luminescent materials; (280.4788) Optical sensing and sensors; (280.6780) Temperature.

References and links

1. L. Qin, Y. Huang, T. Tsuboi, and H. J. Seo, "The red-emitting phosphors of Eu^{3+} - activated $MR_2(MoO_4)_4$ (M = Ba, Sr, Ca; R=La^{3+}, Gd^{3+},Y^{3+}) for light emitting diodes," Mater. Res. Bull. **47**(12), 4498–4502 (2012).
2. M. M. Haque and D.-K. Kim, "Luminescent properties of Eu^{3+} activated $MLa_2(MoO_4)_4$ based (M = Ba, Sr and Ca) novel red-emitting phosphors," Mater. Lett. **63**(9-10), 793–796 (2009).
3. B. S. Barros, A. C. de Lima, Z. R. da Silva, D. M. A. Melo, and S. Alves, Jr., "Synthesis and photoluminescent behavior of Eu^{3+}-doped alkaline-earth tungstates," J. Phys. Chem. Solids **73**(5), 635–640 (2012).
4. V. Bachmann, C. Ronda, and A. Meijerink, "Temperature quenching of Yellow Ce^{3+} luminescence in YAG:Ce," Chem. Mater. **21**(10), 2077–2084 (2009).
5. W. B. Im, N. George, J. Kurzman, S. Brinkley, A. Mikhailovsky, J. Hu, B. F. Chmelka, S. P. DenBaars, and R. Seshadri, "Efficient and color-tunable oxyfluoride solid solution phosphors for solid-state white lighting," Adv. Mater. **23**(20), 2300–2305 (2011).
6. Y. Yang, Q. Zhao, W. Feng, and F. Li, "Luminescent chemodosimeters for bioimaging," Chem. Rev. **113**(1), 192–270 (2013).
7. K. Uheda, N. Hirosaki, Y. Yamamoto, A. Naito, T. Nakajima, and H. Yamamoto, "Luminescence properties of a red phosphor, $CaAlSiN_3 : Eu^{2+}$, for white light-emitting diodes," J. Electrochem. Soc. **9**, H22–H25 (2006).
8. X. Zhang, F. Meng, H. Li, and H. J. Seo, "Synthesis and luminescence of Eu^{3+}-activated molybdates with scheelite-type structure," Phys. Status Solidi **210**, 1866–1870 (2013).
9. P. Benalloul, C. Barthou, and J. Benoit, "$SrGa_2S_4$: RE phosphors for full colour electroluminescent displays," J. Alloy. Comp. **275–277**, 709–715 (1998).
10. C.-H. Kim, I.-E. Kwon, C.-H. Park, Y.-J. Hwang, H.-S. Bae, B.-Y. Yu, C.-H. Pyun, and G.-Y. Hong, "Phosphors for plasma display panels," J. Alloy. Comp. **311**(1), 33–39 (2000).
11. N. Ishiwada, T. Ueda, and T. Yokomori, "Characteristics of rare earth (RE = Eu, Tb, Tm)-doped Y_2O_3 phosphors for thermometry," Luminescence **26**(6), 381–389 (2011).
12. M. D. Chambers, P. A. Rousseve, and D. R. Clarke, "Decay pathway and high-temperature luminescence of Eu^{3+} in $Ca_2Gd_8Si_6O_{26}$," J. Lumin. **129**(3), 263–269 (2009).
13. Y. Cui, H. Xu, Y. Yue, Z. Guo, J. Yu, Z. Chen, J. Gao, Y. Yang, G. Qian, and B. Chen, "A luminescent mixed-lanthanide metal-organic framework thermometer," J. Am. Chem. Soc. **134**(9), 3979–3982 (2012).
14. A. E. Albers, E. M. Chan, P. M. McBride, C. M. Ajo-Franklin, B. E. Cohen, and B. A. Helms, "Dual-emitting quantum dot/quantum rod-based nanothermometers with enhanced response and sensitivity in live cells," J. Am. Chem. Soc. **134**(23), 9565–9568 (2012).
15. B. Lai, L. Feng, J. Wang, and Q. Su, "Optical transition and upconversion luminescence in Er^{3+} doped and Er^{3+}–

Yb^{3+} co-doped fluorophosphate glasses," Opt. Mater. **32**(9), 1154–1160 (2010).
16. X. Wang, J. Zheng, Y. Xuan, and X. Yan, "Optical temperature sensing of $NaYbF_4$: Tm^{3+}@SiO_2 core-shell micro-particles induced by infrared excitation," Opt. Express **21**(18), 21596–21606 (2013).
17. J. P. Feist, A. L. Heyes, and S. Seefelt, "Thermographic phosphor thermometry for film cooling studies in gas turbine combustors," P. I. Mech. Eng. A – J. Pow. **217**, 193–200 (2003).
18. L. C. Bradley, "A temperature-sensitive phosphor used to measure surface temperatures in aerodynamics," Rev. Sci. Instrum. **24**(3), 219–220 (1953).
19. P. Neubert, "Device for indicating the temperature distribution of hot bodies," US Patent no. 2,071.471 (1937).
20. M. M. Gentleman, V. Lughi, J. A. Nychka, and D. R. Clarke, "Noncontact Methods for measuring thermal barrier coating temperatures," Int. J. Appl. Ceram. Technol. **3**(2), 105–112 (2006).
21. H. Peng, M. I. J. Stich, J. Yu, L. N. Sun, L. H. Fischer, and O. S. Wolfbeis, "Luminescent europium(III) nanoparticles for sensing and imaging of temperature in the physiological range," Adv. Mater. **22**(6), 716–719 (2010).
22. S. M. Borisov, A. S. Vasylevska, C. Krause, and O. S. Wolfbeis, "Composite luminescent material for dual sensing of oxygen and temperature," Adv. Funct. Mater. **16**(12), 1536–1542 (2006).
23. H. Kusama, O. J. Sovers, and T. Yoshioka, "Line shift method for phosphor temperature - measurements," Jpn. J. Appl. Phys. **15**(12), 2349–2358 (1976).
24. A. Khalid and K. Kontis, "Thermographic phosphors for high temperature measurements: principles, current state of the art and recent applications," Sensors (Basel Switzerland) **8**(9), 5673–5744 (2008).
25. J. Brübach, C. Pflitsch, A. Dreizler, and B. Atakan, "On surface temperature measurements with thermographic phosphors: A review," Prog. Energ. Combust. **39**(1), 37–60 (2013).
26. M. G. Nikolic, D. J. Jovanovic, V. Dordevic, Z. Antic, R. M. Krsmanovic, and M. D. Dramicanin, "Thermographic properties of Sm^{3+}- doped $GdVO_4$ phosphor," Phys. Scr. T **149**, 1–4 (2012).
27. A. L. Heyes and J. P. Feist, "The characterization of Y_2O_2S:Sm powder as a thermographic phosphor for high temperature applications," Meas. Sci. Technol. **11**(7), 942–947 (2000).
28. J. P. Feist, A. L. Heyes, and J. R. Nicholls, "Phosphor thermometry in an electron beam physical vapour deposition produced thermal barrier coating doped with dysprosium," Proc. Inst. Mech. Eng. Part G J. Aerosp. Eng. **215**(6), 333–341 (2001).
29. V. A. Morozov, A. Bertha, K. W. Meert, S. Van Rompaey, D. Batuk, G. T. Martinez, S. Van Aert, P. F. Smet, M. V. Raskina, D. Poelman, A. M. Abakumov, and J. Hadermann, "Incommensurate modulation and luminescence in the $CaGd_{2(1-x)}Eu_{2x}(MoO_4)_{4(1-y)}(WO_4)_{4y}$ ($0 \le x \le 1$, $0 \le y \le 1$) red phosphors," Chem. Mater. **25**(21), 4387–4395 (2013).
30. W. Zhang, J. Long, A. Fan, and J. Li, "Effect of replacement of Ca by Ln (Ln = Y, Gd) on the structural and luminescence properties of $CaWO_4$:Eu^{3+} red phosphors prepared via co-precipitation," Mater. Res. Bull. **47**(11), 3479–3483 (2012).
31. G. Blasse and B. C. Grabmaier, *Luminescent Materials* (Springer - Verlag, 1994).
32. S. K. Shi, X. R. Liu, J. Gao, and J. Zhou, "Spectroscopic properties and intense red-light emission of (Ca, Eu,M)WO_4 (M = Mg, Zn, Li)," Spectroc. Acta Pt. A-Molec. Biomolec. Spectr. **69**(2), 396–399 (2008).
33. G. Blasse, "The luminescence of closed-shell transition-metal complexes. New developments," *Luminescence and Energy Transfer* (Springer Berlin Heidelberg, 1980), pp. 1–41.
34. S. Alahraché, K. Al Saghir, S. Chenu, E. Véron, D. De Sousa Meneses, A. I. Becerro, M. Ocaña, F. Moretti, G. Patton, C. Dujardin, F. Cussó, J.-P. Guin, M. Nivard, J.-C. Sangleboeuf, G. Matzen, and M. Allix, "Perfectly Transparent $Sr_3Al_2O_6$ Polycrystalline Ceramic Elaborated from Glass Crystallization," Chem. Mater. **25**(20), 4017–4024 (2013).
35. P. A. Tanner, "Some misconceptions concerning the electronic spectra of tri-positive europium and cerium," Chem. Soc. Rev. **42**(12), 5090–5101 (2013).
36. G. Blasse, A. Bril, and W. C. Nieuwpoort, "On the Eu^{3+} fluorescence in mixed metal oxides. Part I - The crystal structure sensitivity of the intensity ratio of electric and magnetic dipole emission," J. Phys. Chem. Solids **27**(10), 1587–1592 (1966).
37. K. Binnemans, "Lanthanide-based luminescent hybrid materials," Chem. Rev. **109**(9), 4283–4374 (2009).
38. Y. Su, L. Li, and G. Li, "Synthesis and Optimum Luminescence of $CaWO_4$-Based Red Phosphors with Codoping of Eu^{3+} and Na^+," Chem. Mater. **20**(19), 6060–6067 (2008).
39. J. Liao, H. You, B. Qiu, H.-R. Wen, R. Hong, W. You, and Z. Xie, "Photoluminescence properties of $NaGd(WO_4)_2$:Eu^{3+} nanocrystalline prepared by hydrothermal method," Curr. Appl. Phys. **11**(3), 503–507 (2011).
40. H. Wu, Y. Hu, W. Zhang, F. Kang, N. Li, and G. Ju, "Sol–gel synthesis of Eu^{3+} incorporated $CaMoO_4$: the enhanced luminescence performance," J. Sol-Gel Sci. Technol. **62**(2), 227–233 (2012).
41. M. G. Nikolić, D. J. Jovanović, and M. D. Dramićanin, "Temperature dependence of emission and lifetime in Eu^{3+}- and Dy^{3+}-doped $GdVO_4$.," Appl. Opt. **52**(8), 1716–1724 (2013).
42. S. A. Wade, "Temperature measurement using rare earth doped fibre fluorescence," phD thesis (Victoria University, 1999).
43. J. A. Capobianco, P. Kabro, F. S. Ermeneux, R. Moncorge, M. Bettinelli, and E. Cavalli, "Optical spectroscopy, fluorescence dynamics and crystal-field analysis of Er^{3+} in YVO_4," Chem. Phys. **214**(2-3), 329–340 (1997).
44. S. F. León-Luis, J. E. Muñoz-Santiuste, V. Lavín, and U. R. Rodríguez-Mendoza, "Optical pressure and temperature sensor based on the luminescence properties of Nd^{3+} ion in a gadolinium scandium gallium garnet crystal," Opt. Express **20**(9), 10393–10398 (2012).
45. E. J. McLaurin, L. R. Bradshaw, and D. R. Gamelin, "Dual-emitting nanoscale temperature sensors," Chem. Mater. **25**(8), 1283–1292 (2013).

#206513 - $15.00 USD Received 19 Feb 2014; revised 7 Apr 2014; accepted 7 Apr 2014; published 22 Apr 2014

46. W. Xu, X. Gao, L. Zheng, Z. Zhang, and W. Cao, "Short-wavelength upconversion emissions in Ho^{3+}/Yb^{3+} codoped glass ceramic and the optical thermometry behavior," Opt. Express **20**(16), 18127–18137 (2012).
47. M. G. Nikolić, V. Lojpur, Ž. Antić, and M. D. Dramićanin, "Thermographic properties of a Eu^{3+} -doped $(Y_{0.75}Gd_{0.25})_2O_3$ nanophosphor under UV and x-ray excitation," Phys. Scr. **87**(5), 055703 (2013).
48. C. D. S. Brites, P. P. Lima, N. J. O. Silva, A. Millán, V. S. Amaral, F. Palacio, and L. D. Carlos, "Thermometry at the nanoscale," Nanoscale **4**(16), 4799–4829 (2012).
49. S. A. Wade, S. F. Collins, and G. W. Baxter, "Fluorescence intensity ratio technique for optical fiber point temperature sensing," J. Appl. Phys. **94**(8), 4743–4756 (2003).
50. C. Eckert, C. Pflitsch, and B. Atakan, "Sol–gel deposition of multiply doped thermographic phosphor coatings Al_2O_3:(Cr^{3+}, M^{3+}) (M = Dy, Tm) for wide range surface temperature measurement application," Prog. Org. Coat. **67**(2), 116–119 (2010).
51. Z. Boruc, M. Kaczkan, B. Fetlinski, S. Turczynski, and M. Malinowski, "Blue emissions in Dy^{3+} doped $Y_4Al_2O_9$ crystals for temperature sensing," Opt. Lett. **37**(24), 5214–5216 (2012).
52. P. Haro-González, I. R. Martín, L. L. Martín, S. F. León-Luis, C. Pérez-Rodríguez, and V. Lavín, "Characterization of Er^{3+} and Nd^{3+} doped strontium barium niobate glass ceramic as temperature sensors," Opt. Mater. **33**(5), 742–745 (2011).
53. D. Jaque and F. Vetrone, "Luminescence nanothermometry," Nanoscale **4**(15), 4301–4326 (2012).

1. Introduction

Scheelites are $A_{1-\square}BO_4$ compounds (A = alkali, alkaline-earth or rare-earth element, B = Mo, W and some other tetrahedrally coordinated cations; $\square$ denotes a cation vacancy) in which broad possibilities of isovalent and heterovalent cation substitutions result in a range of compounds with interesting optical properties, good stability and simple preparation [1–3]. Upon heterovalent substitution at the A sublattice, the charge balance can be maintained by the introduction of cation vacancies, giving rise to compositions characterized by a (A + A'):(BO_4 + B'O_4) ratio different from 1:1. This paper describes the temperature dependent luminescence properties of the $CaGd_{2(1-x)}Eu_{2x}\square(WO_4)_4$ (x = 0 to 1, $\square$ = vacancy) solid solutions and discusses their potential application as a thermographic phosphor.

The technological applications of luminescent materials are very diverse, going from lighting to display and imaging applications [4–10]. In some cases, the luminescence has a very specific temperature dependence, so that it can be used as temperature sensor [11–16]. This was first mentioned by Neubert in 1937 and the first application dates back to the 1950s, when a phosphor was painted on the wing surfaces of a wind-tunnel model in order to probe the temperature of different parts [17–19]. In principle, many different response modes are possible, but the three most important ones are the relative intensities of emission peaks, changes in decay time and shifts in peak position [20–22]. For the presently investigated scheelites, the focus will be on the fluorescence intensity ratio response mode. Kusama et al. were among the first to discuss this technique for $Y_2O_2S:Eu^{3+}$, but the intensity ratios of the Eu^{3+} transitions were insufficiently dependent on the temperature to allow its use as thermographic phosphor [23]. Until now, most research focused on Dy^{3+} or Sm^{3+} as more suitable thermographic rare earth activators, using the temperature dependence of the intensity ratio of different emission lines [24–28]. However, in this paper it will be shown that in the studied scheelite materials, the varying intensity ratio of the emission of the $^5D_0$ and $^5D_1$ energy level of Eu^{3+} is sensitive enough for use as temperature sensor. The mechanism behind the temperature dependence is explained by a phonon-assisted cross-relaxation process, and not by thermalisation like in most cases [4]. To demonstrate the feasibility and prospects of the concept, a patterned resistive heater was coated with $CaEu_2(WO_4)_4$ and illuminated with monochromatic light at 465 nm. The temperature map obtained by using the $^5D_0$ to $^5D_1$ intensity ratio showed high spatial resolution, in addition to an excellent correspondence with the temperature map recorded by more common infrared thermography.

2. Experimental section

Synthesis of the $CaGd_{2(1-x)}Eu_{2x}(WO_4)_4$ solid solutions: a solid state reaction of the tungstates $CaEu_2(WO_4)_4$ and $CaGd_2(WO_4)_4$ was performed. The $CaGd_2(WO_4)_4$ and $CaEu_2(WO_4)_4$ were prepared by heating stoichiometric amounts of $CaCO_3$, WO_3, Eu_2O_3 and Gd_2O_3 at 823 K for 10 h followed by annealing at 1203 K for 96 h in air. Appropriate amounts of $CaEu_2(WO_4)_4$

#206513 - $15.00 USD Received 19 Feb 2014; revised 7 Apr 2014; accepted 7 Apr 2014; published 22 Apr 2014

and $CaGd_2(WO_4)_4$ were mixed to obtain $CaGd_{2(1-x)}Eu_{2x}\square(WO_4)_4$ and subsequently annealed at 1203 K.

Structure Analysis: The phase purity of the obtained $CaGd_{2(1-x)}Eu_{2x}(WO_4)_4$ (x = 0, 0.01, 0.05, 0.1, 0.25, 0.5, 1) solid solutions was checked with X-ray powder diffraction patterns collected on a Thermo ARL X'TRA powder diffractometer (CuKα radiation, λ = 1.5418 Å, Bragg–Brentano geometry, Peltier-cooled CCD detector).

Spectral characterization: Luminescence emission and excitation spectra were obtained with a FS920 spectrometer (Edinburgh Instruments), using a 450W xenon light source, double excitation monochromator and a R928P photomultiplier. All emission and excitation spectra were corrected for the sensitivity of the spectrometer and the intensity of the excitation. Decay times were collected using a pulsed dye laser (λ_{exc} = 385 nm) based on optical pumping by a nitrogen laser (λ_{exc} = 337 nm, pulse duration < 1ns, 1Hz repetition frequency) in combination with an intensified CCD detector (Andor Instruments) coupled to a 0.5 m monochromator. All measurements were taken at room temperature unless mentioned otherwise, and the temperature dependent measurements were performed using an Oxford Optistat CF cryostat.

Thermometry: The resistive heater was made by depositing a thin Al layer by electron beam evaporation onto a AF45 glass substrate (Präzisions Glas & Optik, 5x5 cm^2), through a mask. Some irregularities were introduced in the heater to obtain temperature gradients upon application of a voltage over the outer contacts. Finally, the patterned heater was covered with a thin film of Al_2O_3 (100nm) by e-beam evaporation as a diffusion barrier. To deposit the thermographic phosphor, 0.06 g of $CaEu_2(WO_4)_4$ was mixed with 0.18 g of Silres® (Wacker Chemie), painted on the patterned resistive heater and cured for two hours at 200°C. The material was excited with a Melles Griot argon ion laser with an excitation wavelength of 465 nm. The laser spot was expanded to approximately 3 cm in diameter. Photos were taken with a Nikon D3200 digital camera combined with a 535FS10-M52 green filter (Andover Corporation, transmission peak at 537 nm, 10 nm FWHM) or a red interference filter (peak wavelength of 625 nm) for selecting the green and red emission respectively. To obtain the reference temperature plot a FLIR A35sc (48°) infrared camera was used (320 x 256 resolution, temperature range from –40 °C to 550 °C with an accuracy of ± 5 °C).

3. Results and discussion

3.1 Structural characterization

According to the X-ray powder diffraction, the $CaGd_{2(1-x)}Eu_{2x}(WO_4)_4$ micron-sized powders are single phase and possess a body-centered monoclinically distorted scheelite-type structure. Upon the Gd/Eu substitution, the lattice parameters vary from a = 5.2313(2)Å, b = 5.2436(2)Å, c = 11.4382(4)Å, γ = 90.600(2)^o for x = 0 to a = 5.2365(2)Å, b = 5.2629(2)Å, c = 11.4547(4)Å, γ = 91.152(2)^o for x = 1. Besides the reflections from this basic monoclinic unit cell, satellites are visible on the X-ray powder diffraction patterns. These satellites originate from incommensurately modulated ordering of the A cations and vacancies. The detailed analysis of this modulation is out of scope of this article and is discussed elsewhere [29].

3.2 Luminescence emission and excitation spectra

In Fig. 1(a) the photoluminescence excitation spectrum is shown for $CaGd_{1.8}Eu_{0.2}(WO_4)_4$ upon monitoring the red emission at 612 nm, originating from the $4f^6(^5D_0)$ – $4f^6(^7F_2)$ transition within Eu^{3+}. The excitation spectrum consists of the intraconfigurational $4f^6$-$4f^6$ transitions of Eu^{3+} in the 300 to 500 nm region and a broad band in the region from 250 to 350 nm. The most intense Eu^{3+} 4f-4f excitation peak is due to the $^7F_0$ - $^5L_6$ (395 nm) transition. The small peak at 313 nm corresponds to the $^8S_{7/2}$ - $^6P_{7/2}$ transition within the $4f^7$ configuration of Gd^{3+}. As the $^6P_{7/2}$ level is the lowest excited level of Gd^{3+}, no luminescence is expected from Gd^{3+} due to re-absorption and energy transfer to Eu^{3+}. The presence of the 313 nm peak in the excitation spectrum of the Eu^{3+} emission points to energy transfer between the Gd^{3+} and Eu^{3+} ions. Apart from that, Gd^{3+} has only limited effect on the optical

#206513 - $15.00 USD Received 19 Feb 2014; revised 7 Apr 2014; accepted 7 Apr 2014; published 22 Apr 2014

characteristics, which is common in Eu^{3+}-Gd^{3+} co-doped samples [30, 31]. The excitation spectrum is representative for all studied samples, with composition $CaGd_{2(1-x)}Eu_{2x}(WO_4)_4$ (x = 0.01, 0.05, 0.1, 0.25, 0.5, 1). The broader band peaking at 285 nm is ascribed to a combination of a charge transfer (CT) transition from the 2p orbital of oxygen to the 3d orbital of tungsten in the $(WO_4)^{2-}$ group and an O^{2-} - Eu^{3+} charge transfer band [32–34]. A typical emission spectrum is shown in Fig. 1(b). The most intense emission peak in the region from 600 nm to 620 nm is due to the forced electric dipole transition $^5D_0$ - $^7F_2$. A magnetic dipole emission is found at 590 nm, originating from the $^5D_0$ - $^7F_1$ transition [35]. The emission wavelengths of these 4f-4f transitions are only moderately influenced by the environment of the lanthanide ions since the partially filled 4f shell is well shielded by the filled 5s and 5p orbitals [36, 37]. No additional peaks or shifts in peak positions are observed when varying the europium concentration, only the relative intensities change. For the remainder of this work we will describe the emission originating from the ^5D_J level to the $^7F_{J'}$ ground state multiplet as "^5D_J emission".

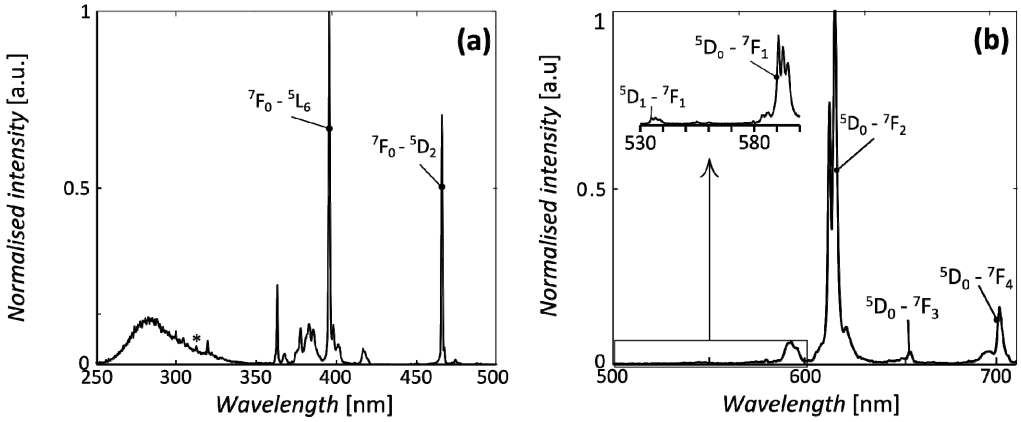

Fig. 1. a) Excitation spectrum of $CaGd_{1.8}Eu_{0.2}(WO_4)_4$ upon monitoring the emission at 612 nm. The excitation peak at 313 nm related to Gd is indicated by (*). b) Emission spectrum of $CaGd_{1.8}Eu_{0.2}(WO_4)_4$ upon excitation at 395 nm. The electronic transitions for the main excitation and emission peaks are indicated.

In Fig. 2 the dependence of the emission intensity of the $^5D_0$ – $^7F_2$ transition on the concentration of Eu^{3+} in $CaGd_{2(1-x)}Eu_{2x}(WO_4)_4$ is illustrated, which can be regarded as a measure for the external quantum efficiency. As can be seen, the intensity reaches a maximum for x = 0.5 and levels off for higher concentrations. Note that the concentration quenching is fairly limited, given the high emission intensity for the fully doped $CaEu_2(WO_4)_4$.

3.3. Decay measurements

The luminescence lifetime of the emission from the different ^5D_J levels was found to be independent of the final level $^7F_{J'}$. At 75 K all samples show a similar mono-exponential decay for the $^5D_0$ emission (λ_{exc} = 385 nm), with a decay constant of 550 µs (Fig. 3), which is in line with previously reported decay times for similar materials [38–40]. For low dopant concentration, the decay profile shows almost no temperature dependence in the 75 K to 475 K range. For the highly doped samples, the temperature dependence is much more pronounced. The sample with full Eu substitution (i.e. $CaEu_2(WO_4)_4$) has a mono-exponential decay profile, but the decay time decreases gradually from 470 µs at low temperature to 230 µs at 475 K.

#206513 - $15.00 USD Received 19 Feb 2014; revised 7 Apr 2014; accepted 7 Apr 2014; published 22 Apr 2014

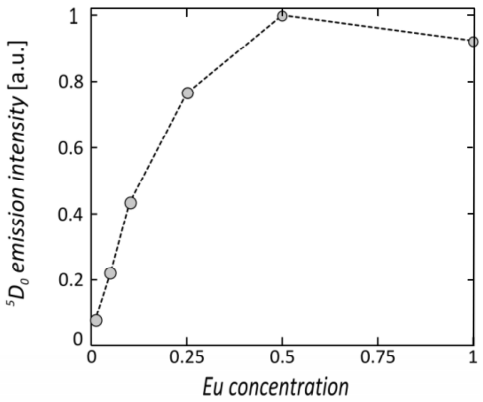

Fig. 2. Concentration dependence of the $^5D_0$ - $^7F_2$ emission intensity in $CaGd_{2(1-x)}Eu_{2x}(WO_4)_4$.

For the intermediate case of $CaGdEu(WO_4)_4$ the decay starts deviating from a mono-exponential profile upon increasing temperature, and an accurate fit can be obtained by combining the low temperature decay component (τ_1 = 550 µs) on the one hand and the changing decay component (τ_2 = 550 µs to 230 µs) of $CaEu_2(WO_4)_4$ at all temperatures on the other hand, in the following way:

$$I(t) = I_1.\exp\left(-\frac{t}{\tau_1}\right) + I_2.\exp\left(-\frac{t}{\tau_2}\right) \quad (1)$$

The fraction of the temperature dependent component in the decay is then defined by:

$$f_2 = \frac{I_2\tau_2}{I_1\tau_1 + I_2\tau_2} \quad (2)$$

and remains constant over the whole temperature range (see Table 1).

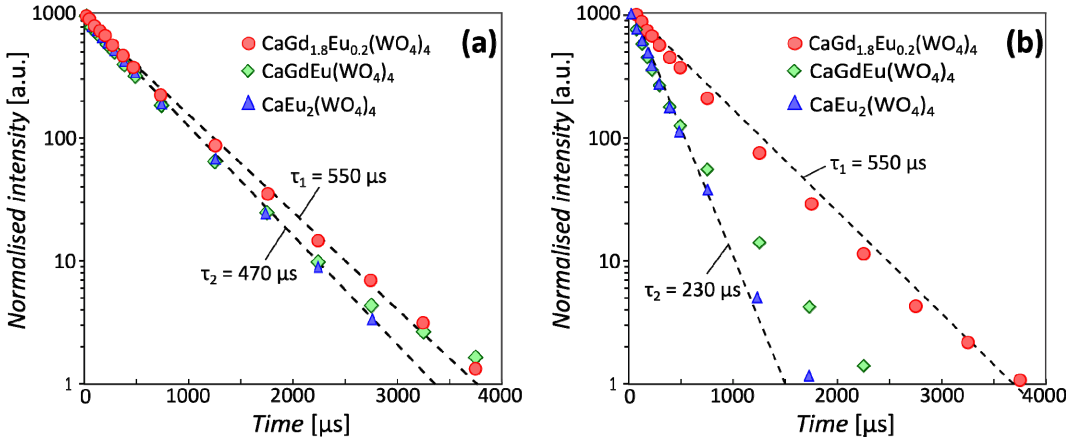

Fig. 3. Decay of the $^5D_0$ emission of $CaGd_{2(1-x)}Eu_{2x}(WO_4)_4$ for x = 0.1,0.5 and 1 at 75K (a) and 475K (b).

Taking into account the limited size difference of Gd^{3+}(r = 1.053 Å) and Eu^{3+}(r = 1.066 Å), we expect both cations to be uniformly distributed in the crystal. For low Eu concentrations this will result in a relatively large average distance between different Eu ions, leading to a low probability of Eu – Eu energy transfer.

#206513 - $15.00 USD Received 19 Feb 2014; revised 7 Apr 2014; accepted 7 Apr 2014; published 22 Apr 2014

Table 1. Decay constant and fraction of the variable decay time component of the $^5D_0$ emission of $CaGd_{2(1-x)}Eu_{2x}(WO_4)_4$

	x = 0.1	x = 0.5	x = 1
75 K	$f_2 = 0$	$f_2 = 0.88$	$f_2 = 1$
	-	$\tau_2 = 470$ µs	$\tau_2 = 470$ µs
300 K	$f_2 = 0$	$f_2 = 0.83$	$f_2 = 1$
	-	$\tau_2 = 280$ µs	$\tau_2 = 280$ µs
475 K	$f_2 = 0.2$	$f_2 = 0.85$	$f_2 = 1$
	$\tau_2 = 230$ µs	$\tau_2 = 230$ µs	$\tau_2 = 230$ µs

As the Gd^{3+} ion is optically silent in the visible part of the spectrum, we can consider the Eu^{3+} ion as an isolated center in the Gd^{3+} dominated host for these low concentrations. For high Eu concentration, energy transfer is likely to occur between the different europium ions and this is obviously the case for the fully substituted $CaEu_2(WO_4)_4$. Interestingly, we can consistently fit the thermal behavior of the decay for different dopant concentrations with only two types of Eu ions (i.e. isolated ones and those showing energy transfer), both characterized by their own specific thermal behavior.

3.4 Thermal quenching

The luminescence spectrum was monitored as a function of temperature in the range from 75 K to 475 K to evaluate the thermal quenching behavior. For the samples with low Eu concentration, the thermal quenching profile of the emission from the ^5D_J levels is quasi-identical for all transitions. The integrated luminescence intensities upon excitation at 465 nm are shown in Fig. 4(a) for $CaGd_{1.8}Eu_{0.2}(WO_4)_4$, with each intensity normalized to the value at 75 K. At a temperature of 300 K, the emission has dropped to 25% of the initial intensity at liquid nitrogen temperature, suggesting that at room temperature a significant fraction of the emission is already quenched. This is somewhat in contrast to the luminescence decay behavior (§3.3), where hardly any decrease of the decay constants was observed upon increasing the temperature. In principle, thermal quenching is accompanied by a faster luminescence decay, due to an increase in non-radiative depopulation of the excited states. This discrepancy could not be explained yet, but might be related to the temperature dependent absorption strength for the excitation light.

Similar to the decay profiles, the temperature dependence of the luminescence is completely different for higher Eu concentrations. The $^5D_0$ emission has similar quenching behavior compared to the samples with low Eu concentration, but for the $^5D_1$ emission a strong absolute increase in intensity is observed for temperatures above room temperature. This is illustrated in Fig. 4(b) for $CaEu_2(WO_4)_4$. For higher Eu concentration the emission output and the decay profiles show a marked temperature dependence and it is therefore expected that energy transfer mechanisms play a role.

In Fig. 5, the decay of the $^5D_1$ emission of $CaEu_2(WO_4)_4$ is depicted and apparently it consists of both a temperature independent component of the order of a microsecond and a temperature dependent slow component. The luminescence decay for Eu^{3+} is commonly much faster for the $^5D_1$ emission than for the $^5D_0$ emission, due to non-radiative depopulation of the higher excited state, e.g. by phonon relaxation or cross-relaxation processes. For higher dopant concentration – and thus for higher probability of energy transfer – the emission from $^5D_1$ is often even not visible at all. Here we observe a fast component in the decay for $^5D_1$ emission with a decay constant of 13 µs for $CaGd_{1.8}Eu_{0.2}(WO_4)_4$ and 1.8 µs for $CaEu_2(WO_4)_4$, which is indeed considerably faster than the $^5D_0$ emission. In addition, an unexpectedly slow component with a decay constant of hundreds of µs is observed as well. By comparing this slow component of the $^5D_1$ emission with the decay of the $^5D_0$ emission at the respective temperatures, a clear correspondence is observed.

#206513 - $15.00 USD Received 19 Feb 2014; revised 7 Apr 2014; accepted 7 Apr 2014; published 22 Apr 2014

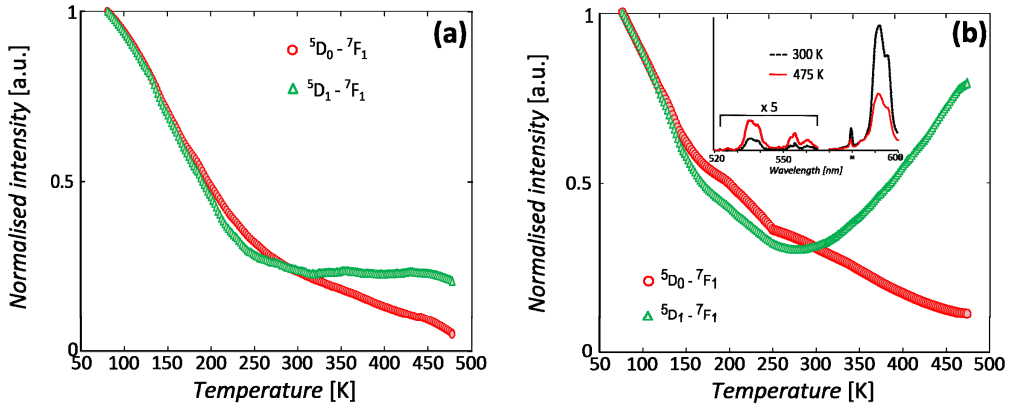

Fig. 4. Temperature dependence of the emission output (λ_{exc} = 465 nm) of the low concentration ($CaGd_{1.8}Eu_{0.2}(WO_4)_4$) (a) and the high concentration ($CaEu_2(WO_4)_4$) (b) samples. The inset shows the emission spectrum at two different temperatures. The intensities are obtained by integrating over the wavelength ranges 535 to 545 nm ($^5D_1$-$^7F_1$) and 585 to 600 nm ($^5D_0$-$^7F_1$).

The fraction of the slow component (defined by Eq. (2)) in the decay of the $^5D_1$ emission varies from $f_2 = 0.3$ at 75 K to $f_2 = 0.8$ at 475 K. This points to an increased feeding of the $^5D_1$ level from the $^5D_0$ level upon increasing temperature for $CaEu_2(WO_4)_4$, by an energy transfer process.

The same decay analysis was performed for $CaGd_{1.8}Eu_{0.2}(WO_4)_4$ (not shown). Although some transfer from $^5D_0$ to $^5D_1$ indeed occurs for these samples, the contribution is too low to result in a considerable increase of the $^5D_1$ emission beyond the normal decay, which can also be observed in Fig. 4(a).

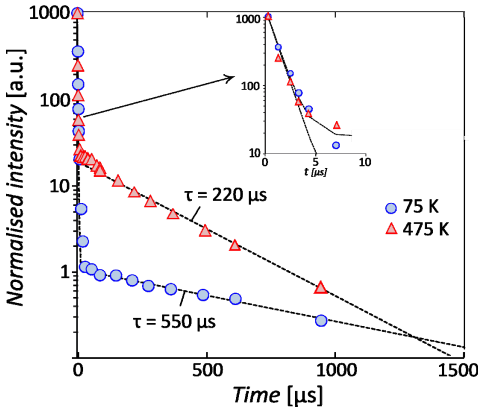

Fig. 5. Decay of the $^5D_1$ emission (λ_{exc} = 385 nm) at 75 K and 475 K for $CaEu_2(WO_4)_4$. The fast decay component remains constant and equals 1.8µs. The slow decay component equals the decay constant of the $^5D_0$ emission at the respective temperatures.

Both the thermal quenching and the decay profiles point at a concentration dependent cross-relaxation process, rather than a simple thermalisation process where the energy difference to populate the $^5D_1$ level from the $^5D_0$ level is fully covered by phonons. As will be substantiated in §3.5, the increase in the $^5D_1$ emission can be explained by a thermally assisted cross-relaxation process with the involvement of two europium ions initially in the excited $^5D_0$ and the $^7F_2$ state:

$$\left(^5D_0\right)_{ion2} + \left(^7F_2\right)_{ion1} + phonons(885cm^{-1}) \longrightarrow \left(^5D_1\right)_{ion2} + \left(^7F_0\right)_{ion1} \qquad (3)$$

#206513 - $15.00 USD Received 19 Feb 2014; revised 7 Apr 2014; accepted 7 Apr 2014; published 22 Apr 2014

This process, depicted in Fig. 6., favors the $^5D_1$ emission of ion 2 (green arrow) at the expense of the $^5D_0$ emission (red arrow), due to the transfer of the $^7F_2 - {}^7F_0$ energy difference from ion 1 (green dotted arrow). As this is not a resonant process, phonons are still needed to overcome the energy difference between $^7F_2 - {}^7F_0$ (1000 cm^{-1} +/– 100 cm^{-1}) and $^5D_0 - {}^5D_1$ (1885 cm^{-1} +/– 100 cm^{-1}). The energy differences between the $^{2S+1}L_J$ manifolds were derived from the emission spectrum. For higher Eu concentrations, this cross-relaxation process is more likely to occur due to a reduced average distance between the Eu ions. Note that a similar temperature dependence was observed for the emission of Eu^{3+} in $GdVO_4$ by Nikolić et al, where the thermal quenching was explained by thermalisation from the lowest to the highest excited level, leading to a thermal barrier of about 1500cm^{-1} [41]. However this thermalisation cannot account for the observed concentration dependence in our case.

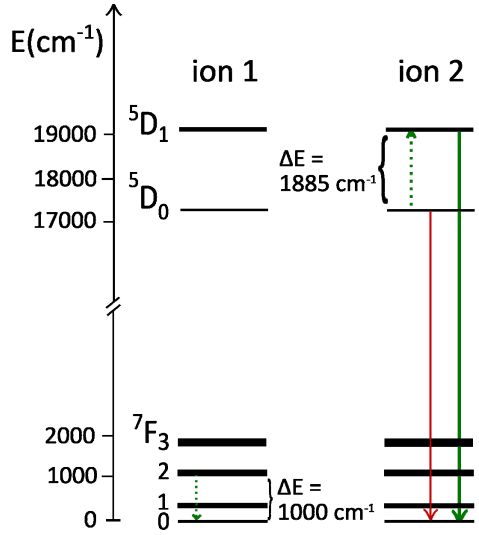

Fig. 6. Eu^{3+} energy level scheme illustrating the phonon-assisted cross-relaxation process.

The involvement of the phonons in Eq. (3) explains for the observed temperature dependence. This thermally assisted cross-relaxation should indeed result in a slow component in the decay of the $^5D_1$ emission, comparable with this for the $^5D_0$ emission, as the energy transfer can only occur as long as the $^5D_0$ level remains populated. Note that the same temperature dependency for the decay constant of the $^5D_0$ emission (Table 1) and the slow component in the $^5D_1$ emission (Fig. 5) is found.

3.5 Use of $CaEu_2(WO_4)_4$ as thermographic phosphor

Because of the strongly changing emission characteristics upon increasing temperature for $CaEu_2(WO_4)_4$, this material is suitable as thermographic phosphor. Figure 7(a) shows the ratio of the $^5D_1$ to $^5D_0$ emission intensity as a function of temperature. The intensities are obtained by integrating over the wavelength ranges 535 to 545 nm ($^5D_1$-$^7F_1$) and 585 to 600 nm ($^5D_0$-$^7F_1$) respectively, upon steady state excitation at 395 nm. However, one is not limited to this excitation wavelength and specific ^5D_J-$^7F_{J'}$ transitions, as the cross-relaxation mechanism only depends on the emitting ^5D_J levels.

Due to the non-resonant character of the cross-relaxation process, the $^5D_0$ and $^5D_1$ energy levels need to be thermally coupled for the process to occur. In case of thermal coupling, it can be shown that the relative population of both levels can be described by a Boltzmann distribution:

$$R = \frac{I_1}{I_0} = B.\exp\left(-\frac{\Delta E}{kT}\right) \quad (4)$$

#206513 - $15.00 USD Received 19 Feb 2014; revised 7 Apr 2014; accepted 7 Apr 2014; published 22 Apr 2014

with B depending on the degeneracy, emission cross-section and angular frequency of the respective levels, k the Boltzmann constant, T the absolute temperature and ΔE the energy difference between the involved states [42–44]. The uncertainty of the experimental data in Fig. 7(a) is on the order of a few degrees Celsius. Measurements were found to be reproducible upon consecutive heating cycles and did not lead to degradation of the material. The Arrhenius plot of the ratio R is given in the inset of Fig. 7(a), and the fit was obtained by varying both B and ΔE. The fitted value of 1068 cm^{-1} for ΔE should be compared with the energy of the phonons needed for the process. This energy is determined by the mismatch between the $^7F_2$ – $^7F_0$ (1000 cm^{-1} +/– 100 cm^{-1}) and $^5D_0$ – $^5D_1$ (1885 cm^{-1} +/– 100 cm^{-1}) energy difference. The variation on each energy difference arises from the multiplet splitting of $^7F_2$ and $^5D_1$. This value agrees reasonably well with the fitted value of 1068 cm^{-1}, so the use of the Boltzmann equation is validated.

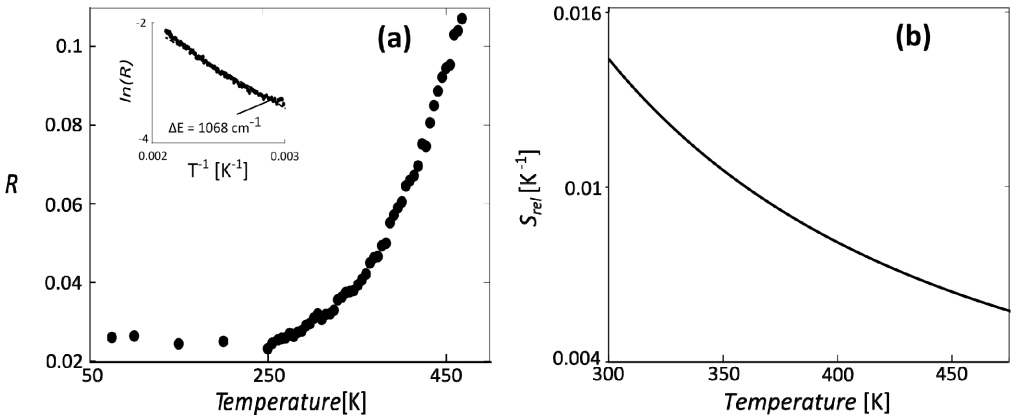

Fig. 7. a) Ratio (R) of the integrated intensities of the $^5D_1$ to $^5D_0$ emission for $CaEu_2(WO_4)_4$ and the corresponding Arrhenius plot (inset). b) Calculated relative sensitivity S_{rel} as a function of temperature.

The one to one correspondence between the data and the fit makes $CaEu_2(WO_4)_4$ applicable as thermographic phosphor from 300 K to at least 500 K. For a quantitative comparison of thermographic phosphors, the relative sensitivity S_{rel} is the most appropriate parameter and is defined as follows [45, 46]:

$$S_{rel} = \frac{1}{R}\frac{dR}{dT} = \frac{\Delta E}{kT^2} \tag{5}$$

The resulting curve is given in Fig. 7(b). The sensitivity varies from 0.014 K^{-1} at 300 K to 0.0047 K^{-1} at 475 K. These values are slightly lower than the relative sensitivities for other Eu^{3+} doped thermographic materials. For example Eu^{3+} doped $(Y_{0.75}Gd_{0.25})_2O_3$ has a maximum relative sensitivity of 0.025K^{-1} [47]. On the other hand, the scheelite thermographic phosphor has a much larger temperature operation range compared to most self-referencing materials [48]. Compared to the performance of Dy^{3+}, Sm^{3+} and Nd^{3+} doped materials or up-conversion nano-particles, the obtained maximum sensitivity is similar or even higher [27, 47–53].

To prove its usefulness in thermal imaging, $CaEu_2(WO_4)_4$ phosphor powder was mixed in a 1:3 weight ratio with SILRES® binder and coated onto a patterned, purposely made resistive heater (Fig. 8) to obtain an inhomogeneous temperature distribution. The device was heated to a maximum local temperature of about 150°C. Then, the coated heater was illuminated with the 465 nm emission of an Ar laser to excite Eu^{3+} via the $^7F_0$-$^5D_2$ transition. In order to map the temperature gradients of the heated surface, pictures were taken with a Nikon D3200 digital reflex camera combined with a green and a red narrow band filter,

#206513 - $15.00 USD Received 19 Feb 2014; revised 7 Apr 2014; accepted 7 Apr 2014; published 22 Apr 2014

collecting the relevant fractions of the green $^5D_1$ and the red $^5D_0$ emission separately. Images were read out in the NEF data format, and divided pointwise. Using Eq. (4), a thermal map was obtained (Fig. 8, middle). As a reference, images were made with a thermal imaging

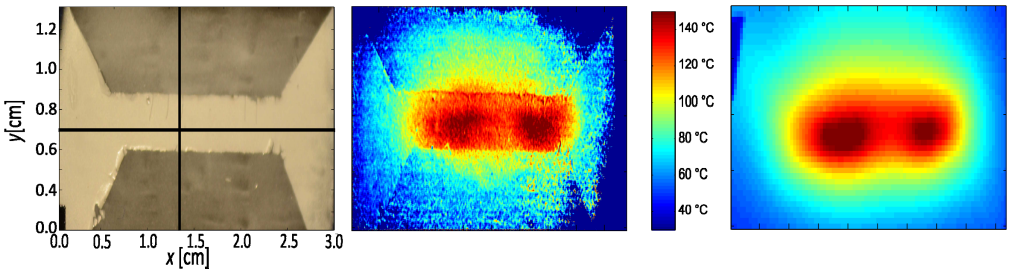

Fig. 8. Patterned resistive heater with cross-sections for the vertical and horizontal profile indicated by the black lines (left). Temperature plot of the patterned resistive heater, imaged with the use of the thermographic phosphor (middle) and with an infrared camera (right).

infrared camera (Fig. 8, right). For both types of measurements, a horizontal and a vertical temperature profile was extracted from the corresponding thermal maps (Fig. 9) at the positions indicated on the photograph of the coated heater (Fig. 8, left). It can be seen that the thermographic scheelite phosphor is capable of reproducing the temperature gradients in a very accurate way, which proves the applicability of the material in the postulated temperature range.

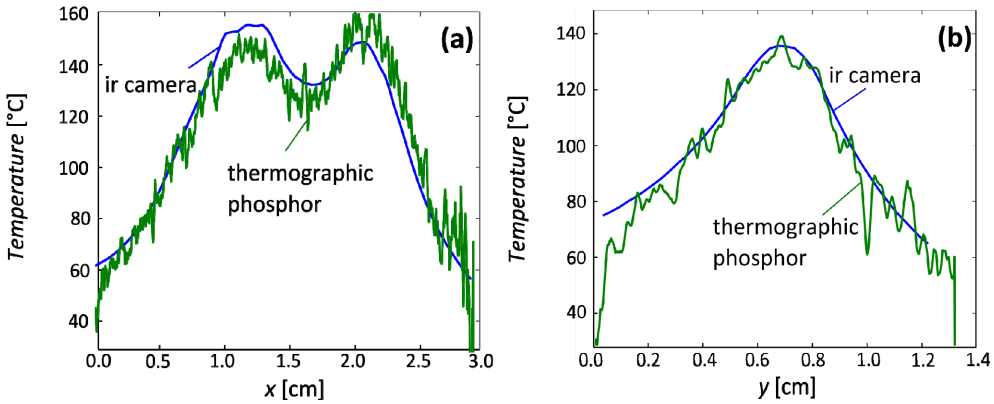

Fig. 9. Horizontal (a) and vertical (b) temperature profiles extracted from the temperature plots in Fig. 8.

A major advantage specific for this response mode is that there is no need for an absolute intensity measurement, eliminating errors introduced by fluctuations in excitation intensity and light collection efficiency [45]. Together with the obtained high spatial resolution and the non-destructiveness of the method, this makes the material a very promising candidate for thermometry. Indeed, after use, the phosphor coating can be easily removed using an appropriate solvent such as acetone. In addition, the involved emission peaks are very well separated, making the detection relatively easy. The main drawback for the material is the low $^5D_1$ emission intensity compared to the $^5D_0$ emission intensity. Nevertheless, the cross-relaxation process can still be optimized, for example by minimizing the defects in the host material. This reduces the non-radiative decay paths from $^5D_0$ to ^7F_J, which can then increase the probability of populating the $^5D_1$ level. In addition, other host materials could be chosen with a different distance between the europium ions or with phonon energies having an improved match with the energy needed for the cross-relaxation process.

#206513 - $15.00 USD Received 19 Feb 2014; revised 7 Apr 2014; accepted 7 Apr 2014; published 22 Apr 2014

4. Conclusion

In this work, we investigated the temperature dependence of both the luminescence and the decay pathways of $CaGd_{2(1-x)}Eu_{2x}(WO_4)_4$ scheelites in a systematic way. All phosphors emit intense red light dominated by the $^5D_0 - {}^7F_2$ transition at 612 nm, and have similar excitation and emission spectra. The temperature dependence of the ^5D_J emission intensities was however found to be strongly dependent on the europium concentration. For high Eu concentration strong cross-relaxation occurred upon increasing temperature due to energy transfer between nearby Eu ions. This thermally assisted cross-relaxation manifests itself in an increasing emission from the $^5D_1$ level, characterized by the same decay time as the $^5D_0$ emission, upon increasing temperature. Because of this specific temperature dependence, $CaEu_2(WO_4)_4$ was proven to be suitable for intensity ratio based temperature measurements. The ratio of the $^5D_1$ to $^5D_0$ emission intensity follows a Boltzmann distribution equation. Consequently, an accurate estimate of the temperature can be made in the range from 300 K to at least 500 K by measuring the relative emission intensity of both peaks. This temperature range is large compared to other ratiometric systems and it was experimentally shown that the phosphor was able to reproduce temperature gradients with high accuracy and spatial resolution, confirming the applicability of the material for thermometry and thermography. A disadvantage of the present phosphor is the relatively low integrated emission intensity from the $^5D_1$ emission compared to the dominating $^5D_0$ emission, which lengthens the acquisition time for the thermal imaging. Future work will therefore focus on the optimization of the cross-relaxation process and the total emission intensity of the $^5D_1$ state, by optimizing the host composition and reduction of the non-radiative decay paths.

Acknowledgment

This research was supported by FWO (projects G039211N, G006410), Research Foundation - Flanders. V.M. is grateful for financial support of the Russian Foundation for Basic Research (Grants 08-03-00593, 11-03-01164, and 12-03-00124). We gratefully thank Mathias Helsen and Jonas Botterman for assisting in the measurements.

#206513 - $15.00 USD Received 19 Feb 2014; revised 7 Apr 2014; accepted 7 Apr 2014; published 22 Apr 2014